Fractional power-law behavior and its origin in iron-chalcogenide and ruthenate superconductors: Insights from first-principles calculations

Z. P. Yin,* K. Haule, and G. Kotliar

Department of Physics and Astronomy, Rutgers University, Piscataway, New Jersey 08854 USA

(Received 23 August 2012; revised manuscript received 15 November 2012; published 29 November 2012; corrected 11 December 2012)

We perform realistic first-principles calculations of iron chalcogenides and ruthenate-based materials to identify experimental signatures of Hund's-coupling-induced correlations in these systems. We find that FeTe and $K_xFe_{2-y}Se_2$ display unusual orbital-dependent fractional power-law behavior in their quasiparticle self-energy and optical conductivity, a phenomenon first identified in $SrRuO_3$. Strong incoherence in the paramagnetic state of these materials results in electronic states hidden to angle-resolved photoemission spectroscopy which reemerge at low temperatures. We identify the effective low-energy Hamiltonian describing these systems and show that these anomalies are not controlled by the proximity to a quantum critical point but result from coexistence of fast quantum mechanical orbital fluctuations and slow spin fluctuations.

DOI: 10.1103/PhysRevB.86.195141 PACS number(s): 74.20.Pq, 74.25.Gz, 74.25.Jb, 74.70.−b

I. INTRODUCTION

The study of the Hund's coupling effects in solids has a long history. Van der Marel and Sawatsky[1] pointed out that, unlike the Hubbard U which is strongly screened, the atomic Hund's J_H persists essentially unrenormalized in the solids and increases the splittings between the lower and the upper Hubbard bands for a half-filled shell, while decreasing it away from half filling. The Hund's term was also shown to have important consequences on the low-energy physics of quasiparticles, when a transition metal impurity is screened in a metallic host. The Hund's coupling was shown to dramatically reduce the value of the Kondo temperature.[2,3] Recent interest in this problem arose from dynamical mean-field theory[4] (DMFT) investigations of the recently discovered iron-pnictide superconductors. It was proposed that in these materials strong correlations arise from the Hund's rule coupling J_H,[5] rather than from the Hubbard U, resulting in large mass enhancements. These calculations[5] showed that for a reasonable value of the Hubbard U, the mass enhancement due to interactions is very small when $J_H = 0$, whereas it is exponentially enhanced by the Hund's rule coupling. Optical spectroscopy studies have shown that in both iron pnictides and chalcogenides the optical masses are many times larger than the band masses.[6–9] The trend in mass enhancements is well accounted for by DMFT combined with density functional theory (DFT) calculations.[10] Since the strength of correlations in these solids is almost entirely due to the Hund's coupling, these materials are dubbed Hund's metals.[10] The role of Hund's coupling in iron pnictides and chalcogenides has been addressed from different perspectives in the literature.[10–26] Power-law behavior in the quasiparticle self-energy of model Hamiltonians with Hund's coupling was discovered in Ref. 27 and related to observations in ruthenates.[28,29] Many anomalous properties of ruthenates[30] and other 4d compounds were shown to be governed by Hund's physics.[31]

While at low energies and low temperatures Hund's metals are describable by Fermi liquid theory, the physical properties in their incoherent regime are anomalous and surprising. In the iron pnictides and chalcogenides there is a strong tendency towards orbital differentiation,[10] and the large mass enhancement can occur even though no clear Hubbard band exist in the one-particle spectra of these Hund's metals.[32]

In this article, we use first-principles methods and model Hamiltonians to search for experimental signatures of Hund's physics in iron chalcogenides and ruthenates, which are the subject of current intensive experimental studies. We show how the incoherence in iron chalcogenides above the Néel temperature can blur portions of the Fermi surface, rendering them dark to photoemission spectroscopy. We show that the fractional power-law behavior in optical conductivity that received significant attention in the ruthenates also takes place in the FeTe system, deepening the analogies between these systems. We compare the power-law exponents in optical conductivity extracted from first-principles DFT + DMFT calculations with experiments in a broad class of materials, and elucidate the control parameters that govern this behavior. The fractional power-law behavior is characteristic of an intermediate regime where the orbital degrees of freedom are quenched but the spin degrees of freedom are not. This physics is most pronounced at the special valence of one unit of charge away from half filling.

II. RESULTS

A. DFT + DMFT results

We first show results of our realistic DFT + DMFT calculation[33,34] for three compounds currently under extensive investigations: the ruthenates Sr_2RuO_4 and the iron chalcogenides FeTe and $K_xFe_{2-y}Se_2$. In all the DFT + DMFT calculations, we use the same Coulomb repulsion $U = 5.0$ eV and Hund's $J_H = 0.80$ eV, as determined *ab initio* in Ref. 32, and used in our previous work.[10,12] Notice that we include all the electronic states in a large energy window (−10 to 10 eV) as opposed to three- or five-band model calculations; thus the Hubbard U appropriate for our calculations is much less screened than in those studies. The electronic charge is computed self-consistently on the DFT + DMFT electronic density. The quantum impurity problem is solved by the continuous-time quantum Monte Carlo (CTQMC) method,[35,36] using the Slater form of the Coulomb repulsion in its fully rotationally invariant form. We use the experimentally

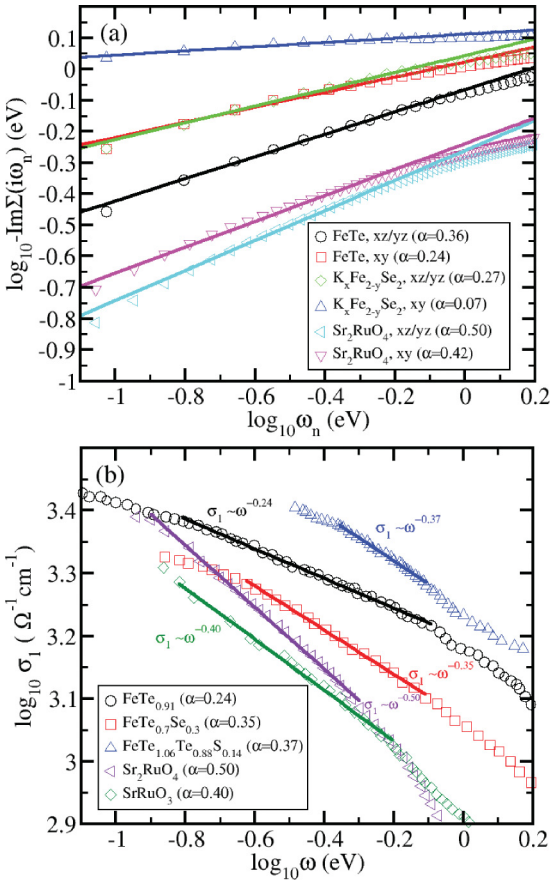

FIG. 1. (Color online) Fractional power law in (a) theoretical self-energy and (b) experimental optical conductivity in iron chalcogenides and ruthenates. Experimental data are taken from Ref. 42 for $FeTe_{0.91}$ and $FeTe_{0.7}Se_{0.3}$, Ref. 43 for $Fe_{1.06}Te_{0.88}S_{0.14}$, Ref. 28 for Sr_2RuO_4, and Ref. 29 for $SrRuO_3$.

determined lattice structures, including the internal positions of the atoms for Sr_2RuO_4,[37] FeTe,[38] $K_xFe_{2-y}Se_2$,[39] and FeSe.[40]

We show in Fig. 1(a) the imaginary part of the self-energy of the t_{2g} orbitals in Sr_2RuO_4, FeTe, and $K_xFe_{2-y}Se_2$ on the imaginary axis, plotted in $\log_{10}$ scale. In the intermediate energy range from a low-energy cutoff ~0.1 eV, below which the materials gain coherence, to roughly Hund's $J_H \sim 0.8$ eV, the imaginary part of the self-energy clearly shows a fractional power-law behavior, i.e., $\mathrm{Im}\Sigma(i\omega_n) \propto -\omega_n^{\alpha}$. For the normal Fermi liquid, this exponent is unity, and at finite temperature correlated materials have an additional constant scattering rate. The fractional powerlaws are however very uncommon.

From the quantum chemistry perspective, both iron chalcogenides and ruthenates share a common theme: they contain correlated electrons with the d valence of one unit charge away from half filling. In iron pnictides (chalcogenides), the Fe ion is surrounded by a tetrahedron of pnictogen (chalcogen), and the resulting crystal field splittings are very small compared to Fe-pnictogen hybridization;[5] hence all five Fe $3d$ orbitals are active. Their average occupancy is close to d^6, one unit of charge away from the half-filled d^5. For the ruthenates, the coordination of the Ru is octahedral, and the oxygen ligands induce a large t_{2g}-e_g splitting, with only the t_{2g} orbitals active, containing approximately four electrons in three t_{2g} orbitals, one electron more than in the half-filled shell.

The values of the apparent power-law exponents differ from material to material and deviate even for different orbitals of the same material, which is connected to the orbital occupancy. As shown in Fig. 1(a), the xz and yz orbitals of Sr_2RuO_4 show an exponent of 0.5, while the more correlated xy orbital, which is closer to half filling, show a smaller exponent of 0.42. In iron pnictides and chalcogenides, the average occupancy per orbital is even closer to half filling (only 1/5 away, as opposed to 1/3 in ruthenates). As we will show below by a model study, one expects stronger electronic correlations in this case and a smaller power-law exponent. Indeed, the xz and yz orbitals in FeTe show an exponent of ≈0.36, whereas for the more strongly correlated xy orbital, the exponent is only ≈0.24. Iron vacancies in $K_xFe_{2-y}Se_2$ make the compound even more correlated than FeTe, and the power-law exponent is further reduced to 0.27 for the xz and yz orbitals, and to only 0.07 for the xy orbital.

The power-law behavior of the self-energy manifests itself in optical conductivity studies. In a simplified treatment, the optical conductivity can be approximated by $\sigma(\omega) \propto \mathrm{Re}\{1/[\omega + i\Sigma''(\omega) + \Sigma'(\omega) - \Sigma'(\omega = 0)]\}$.[41] In Fig. 1(b), we present experimental data on $FeTe_{0.91}$,[42] $FeTe_{0.7}Se_{0.3}$,[42] $Fe_{1.06}Te_{0.88}S_{0.14}$,[43] Sr_2RuO_4,[28] and $SrRuO_3$.[29] As can be seen in Fig. 1(b), the optical conductivity in these materials can be roughly approximated by $\sigma_1(\omega) \sim B\omega^{-\alpha}$ in about the same energy range as the theoretical self-energy. The experimental exponents obtained from optical conductivity are very similar to the theoretical exponents for the self-energy, as expected from the simplified relation between optical conductivity and self-energy.

Hund's metals have a very low temperature scale, called the coherence temperature, below which a Fermi-liquid-like coherence regime is reached. This phenomenon has been discussed in other contexts such as heavy fermions[44,45] and transition metal oxides[46] and can be fruitfully probed by photoemission spectroscopy. At finite temperatures, some electronic states can be very incoherent, and coherence in different electronic states is usually not reached simultaneously. Due to the strong orbital differentiation discussed in Ref. 10, the t_{2g} orbitals have lower coherence temperature than the e_g orbitals in the iron-based superconductors. Within the t_{2g} shell, the xy orbital has the lowest coherence temperature. In Fig. 2 we show the gradual evolution of the Fe t_{2g} orbitals from a very incoherent state at high temperature to a partially coherent state at lower temperature in paramagnetic (PM) state of FeTe. We display the momentum- and orbital-resolved density of electronic states at temperatures of 387, 232, 116, and 58 K. For comparison, we also show the momentum-resolved density of states of PM FeSe at 116 K, where all electronic states are quite coherent. The buildup of coherence in the orbitally resolved spectra of FeTe is seen as a gradual buildup of the quasiparticle peak from a broad hump at elevated temperature to a sharper peak at lower temperature in Figs. 2(e) and 2(f). In momentum space, the coherence is achieved more unevenly. While some bands can be identified at 116 K, and become pretty sharp at 58 K, other bands are barely noticeable even at 58 K. In particular, the band of primarily xy character circled

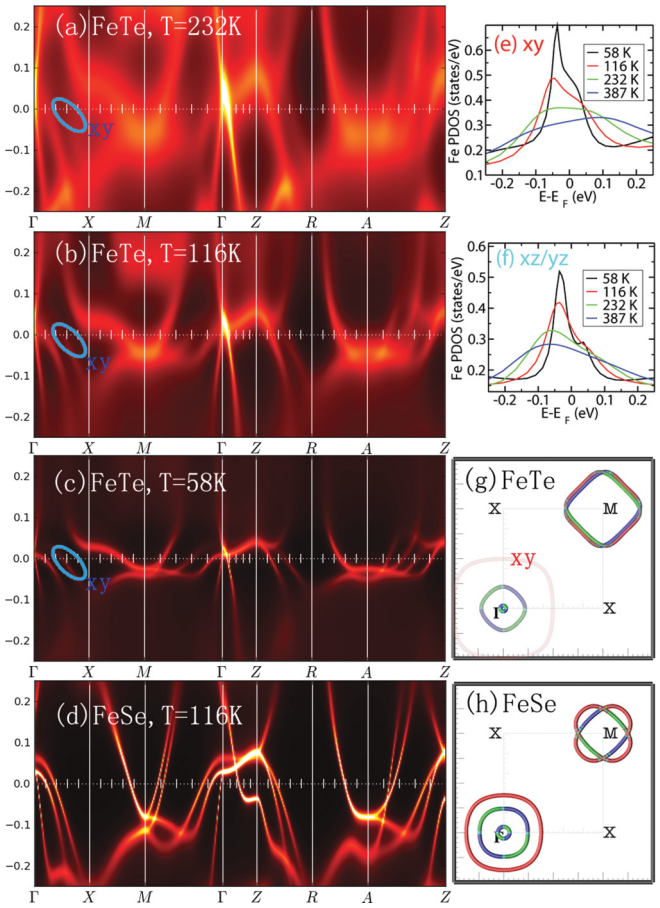

FIG. 2. (Color online) Incoherence-coherence crossover in FeTe. $A(\mathbf{k},\omega)$ along the path $\Gamma \to X \to M \to \Gamma \to Z \to R \to A \to Z$ for FeTe at (a) 232 K, (b) 116 K, and (c) 58 K and for (d) FeSe at 116 K in the PM states. (e), (f) $A(\omega)$ for the Fe $3d$ xy and the xz and yz orbitals at 387, 232, 116, and 58 K in PM FeTe. (g), (h) Color-coded Fermi surface in the Γ plane for PM FeTe and FeSe, respectively. Red, green, and blue colors correspond to xy, xz, and yz orbital character, respectively. Due to the incoherent nature of the xy orbital above T_N, the outer hole pocket around Γ is not easy to detect in ARPES experiments.

by the blue ellipse has an enormous scattering rate at 58 K and should be hard to detect by angle-resolved photoemission spectroscopy (ARPES). The missing Fermi surface is drawn in Fig. 2(g) as a large red pocket centered at the Γ point, which is very incoherent above T_N, and hence is missing in the photoemission of the paramagnetic FeTe, in strong contrast to paramagnetic FeSe [Fig. 2(h); see also Ref. 47]. Our calculation shows that K-intercalated FeSe ($K_xFe_{2-y}Se_2$) is even more correlated than FeTe, and has smaller power-law exponents and lower coherence temperature than FeTe. This is in agreement with recent angle-resolved photoemission spectroscopy experiments on $A_xFe_{2-y}Se_2$ compounds (A = K, Rb, Cs) where an orbital-dependent incoherence-coherence crossover was observed by Yi and collaborators.[48]

B. Low-energy Hamiltonian

To gain some understanding of the Hund's physics in these systems, we derive below a low-energy Hamiltonian of the three-band Hubbard model, the simplest model which shows power-law behavior of the self-energy. The starting Hubbard Hamiltonian is $H = H_t + H_U$, with the hopping term $H_t = \sum_{ij\sigma,a,b} t_{ab}^{ij} f_{ia\sigma}^{\dagger} f_{jb\sigma}$ and Coulomb term $H_U = \frac{1}{2}\sum_{i\sigma,abcd} U[a,b,c,d] f_{ia\sigma}^{\dagger} f_{ib\sigma'}^{\dagger} f_{ic\sigma'} f_{id\sigma}$. Here a,b,c,d (i,j) are orbital (site) indices, and σ stands for the spin. The hopping term is taken to be locally SU(6) symmetric (no crystal fields), while the Coulomb interaction is set to $U[a,b,c,d] = U\delta_{ad}\delta_{bc} + J\delta_{ac}\delta_{bd}$, which reduces the symmetry to SU(3) × SU(2). Within DMFT, this model maps to an SU(3) × SU(2) impurity Hamiltonian. To understand why the Hund's rule coupling has such a dramatic effect on the physical properties, we first perform a Schrieffer-Wolff transformation (for its derivation, see the Appendix) to obtain a Kondo-like Hamiltonian, of the form $H_{\rm eff}^{\rm Kondo} = H_0 + H_1 + H_2 + H_3$, with the potential scattering term $H_0 = J_p \sum_{a\sigma} \psi_{a\sigma}^{\dagger}(0)\psi_{a\sigma}(0)$, the spin-spin Kondo part $H_1 = J_1 \sum_{\alpha} S^{\alpha} \sum_{a\sigma\sigma'} \psi_{a\sigma}^{\dagger}(0)\sigma_{\sigma\sigma'}^{\alpha}\psi_{a\sigma'}(0)$, the orbital-Kondo part, $H_2 = J_2 \sum_{\alpha} T^{\alpha} \sum_{ab\sigma} \psi_{a\sigma}^{\dagger}(0)\lambda_{ab}^{\alpha}\psi_{b\sigma}(0)$, and the coupled spin-orbital part $H_3 = J_3 \sum_{\alpha\beta} T^{\alpha} S^{\beta} \sum_{ab\sigma} \psi_{a\sigma}^{\dagger}(0)\lambda_{ab}^{\alpha}\sigma_{\sigma\sigma'}^{\beta}\psi_{b\sigma'}(0)$. Here $S^{\alpha} = \sum_{a\sigma\sigma'} f_{a\sigma}^{\dagger} \frac{1}{2}\sigma_{\sigma\sigma'}^{\alpha} f_{a\sigma'}$ and $T^{\beta} = \sum_{ab\sigma} f_{a\sigma}^{\dagger}\lambda_{ab}^{\beta} f_{b\sigma'}$ are spin and SU(3) orbital operators acting on the impurity site, $\psi(0)$ are field operators of the conduction electrons coupled to the impurity, while $\sigma_{\sigma\sigma'}^{\alpha}$ and λ_{ab}^{α} are Pauli matrices and the Gell-Mann 3 × 3 matrices of the SU(3) group, respectively.

Notice that in our picture the same electrons carry both orbital and spin degrees of freedom, in contrast to the point of view of Ref. 49, which emphasizes the spin and orbital degrees of freedom being carried by different type of electrons, i.e., t_{2g} the spin, and e_g the orbital.

While the form of the low-energy impurity model is dictated by symmetry considerations, the exchange couplings J_1, J_2, J_3 depend crucially on the impurity valence and Hund's coupling J_H. For the half-filled shell and large J_H, only the spin-spin term J_1 survives, and a well-known reduction of the J_1 Kondo coupling for a factor of $(2l+1)$ was derived in Refs. 2 and 3 compared to a corresponding one-band model. Consequently, a huge reduction of the Kondo temperature for a factor of $(2l+1)^2$ in the exponent was derived in Ref. 3. This regime is relevant for the half-filled d^5 shell realized in the Hund's insulators LaMnPO.[50]

For the above Hund's metals, the relevant valence of the transition metal ion is one unit of charge away from half filling. When J_H is negligible, the Hamiltonian is SU(6) symmetric, and all three Kondo couplings J_1, J_2, J_3 are positive (antiferromagnetic). For the valence $n_{\rm imp} = 2$ (or $n_{\rm imp} = 4$), their numerical values are $J_1 = J_0/3$, $J_2 = J_0/4$, and $J_3 = J_0/2$, where $J_0 = V^2/(2U + \varepsilon_f)$ [or $J_0 = V^2/(3U + \varepsilon_f)$] is a positive number, which depends on the corresponding Anderson impurity model parameters, i.e., hybridization V and impurity level ε_f. The ground state is a Fermi liquid, because antiferromagnetic couplings between conduction electrons and impurity degrees of freedom ensure complete quenching of both the orbital and spin moments. On the other hand, when J_H is large, the spin-spin Kondo coupling J_1 changes sign to ferromagnetic, while the orbit J_2 and spin-orbit J_3 couplings remain positive. In the three-band SU(2) × SU(3) model and for large J_H, their

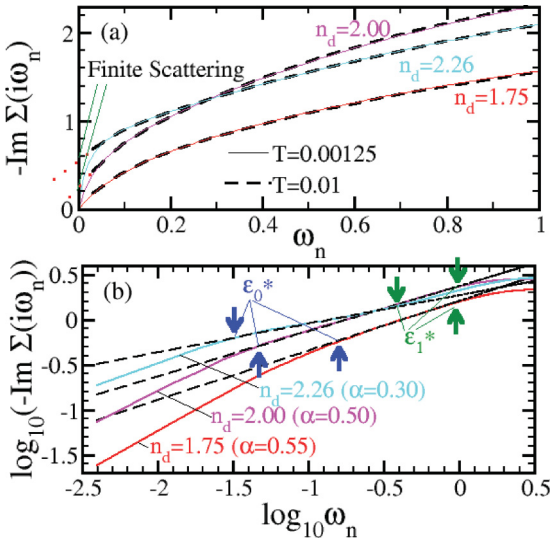

FIG. 3. (Color online) Quasiparticle self-energies for a three-band model with $J_H = 2.0$ at different fillings $n_d = 1.75$, 2.00, and 2.26. (a) The self-energies at two temperatures $T = 0.01$ and 0.001 25 show the incoherence-coherence crossover with decreasing temperature. (b) The self-energies plotted in $\log_{10}$ scale display fractional power-law behavior in the intermediate frequency range from ε_0^* to ε_1^* as indicated by arrows.

numerical values are $J_1 = -J_0/9$, $J_2 = J_0/3$, and $J_3 = J_0/3$, where $J_0 = V^2/(2U - 2J_H + \varepsilon_f) > 0$ [or $J_0 = V^2/(3U + J_H + \varepsilon_f) > 0$] for valence $n_{\rm imp} = 2$ (or $n_{\rm imp} = 4$). This change of sign is due to the orbital blocking mechanism,[10] which allows only those virtual charge excitations that go through an orbital singlet intermediate state (see the Appendix). We note that for valence d^6 in iron pnictides and chalcogenides, the correct low-energy Hamiltonian has three terms, not just the spin-spin term, as proposed earlier.[51] It is, however, the spin-spin J_1 term that changes sign in the limit of large J_H, and impedes quenching of the spin degrees of freedom (termed spin freezing in Ref. 27). This substantially reduces the coherence temperature; however, the J_3 term, which couples spin and orbital, is positive and gives rise to the Fermi liquid state at very low temperature.

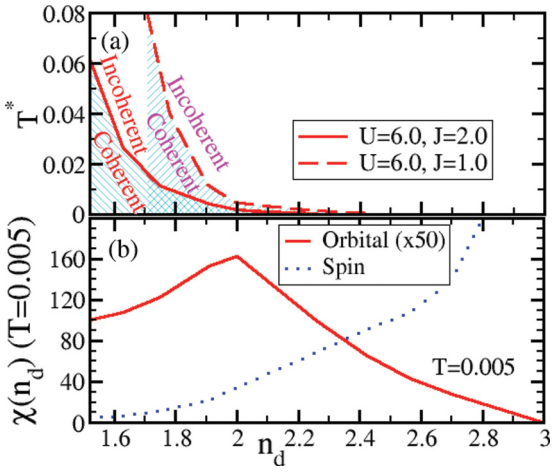

FIG. 4. (Color online) (a) The coherent temperature and (b) the spin and orbital susceptibility, as functions of n_d for a three-band model with $J_H = 2.0$ (solid lines) and $J_H = 1.0$ (dashed lines).

C. Model Hamiltonian calculations

To demonstrate the above picture, we numerically solve a simplified three-band model with the nearest-neighbor diagonal hopping $t_{\alpha\alpha} = 0.4$, and the next-nearest-neighbor hopping $t'_{\alpha\alpha} = 0.4$ and $t'_{\alpha\neq\beta} = 0.2$, which give a total bandwidth of the tight-binding model $W \approx 3.5$. We take $U = 6$ and large Hund's coupling $J_H = 2$ and $J_H = 1$ for the power law to extend over a larger frequency range.

In Fig. 3(a), we show the imaginary part of the quasiparticle self-energies for $J_H = 2$. At the intermediate temperature $T = 0.01$, the self-energies of $n_d = 2.00$ and 2.26 display finite values at zero frequency by extrapolation, which suggests incoherent properties at this temperature. However, at a lower temperature $T = 0.001\,25$, the corresponding self energies clearly display Fermi liquid behavior at low frequencies. Therefore there is an incoherence-coherence crossover with decreasing temperature. We determine the coherence temperature as the temperature at which the renormalized scattering rate is equal to the temperature, i.e., $-z{\rm Im}\Sigma(i\omega = i0^+, T^*) = k_B T^*$, where $1/z = 1 - \partial{\rm Im}\Sigma(i\omega = i0^+, T^*)/\partial\omega$ and k_B is the Boltzmann constant. We show the coherent temperature in Fig. 4(a) as a function of electron occupation n_d. We reached an eight-times lower temperature than previous studies[27] to access the Fermi liquid state at filling far beyond $n_d = 2$, and map out the coherence-incoherence crossover temperature T^*.

A good power-law fit to the self-energy, as shown in Fig. 3(b), is obtained only in a limited range of frequency between the low-energy cutoff proportional to the Fermi liquid scale [ε_0^* in Fig. 3(b)] and the high-energy cutoff (ε_1^*), which is always smaller than the Hund's coupling. The range of frequencies at which the power law is valid [$\varepsilon_0^* < \omega_n < \varepsilon_1^*$, as indicated by arrows in Fig. 3(b)] is largest at valence $n_d = 2$, where the exponent is close to 1/2, as previously reported in Ref. 27. The much lower temperatures reached in this work show that the exponent α decreases monotonically with increasing n_d [see Fig. 3(b) and Figs. 5 and 6 in the Appendix], in contrast to Ref. 27; hence stronger correlations approaching the Mott state at $n_d = 3$ lead to smaller exponents at low temperatures, in qualitative agreement with our realistic calculations for Fe and Ru compounds. Most importantly, there is no signature of a quantum phase transition to a non-Fermi-liquid spin-frozen state around valence $n_d = 2$, where the power-law exponents are found, and the crossover temperature scale does not follow the power-law behavior $T^* \sim (x - x_c)^{z\nu}$ expected in a quantum critical scenario. Hence we can *exclude* the possibility that the exponents are due to the proximity to the quantum phase transition, as proposed in Refs. 27 and 52.

III. DISCUSSION

The power-law exponents are found in the temperature and frequency regime where the spin degrees of freedom are very slow and unquenched (the spin susceptibility has Curie-Weiss form and a large static value) while the orbital degrees of freedom are very fast and quenched (the orbital susceptibility is Pauli-like, but enhanced) [see Fig. 4(b) and Fig. 7 in the Appendix] This is an interesting regime in which two degrees of freedom behave in different ways, one fluctuating very fast (positive J_2), the other very slowly

(negative J_1), and both coupled by a third antiferromagnetic coupling J_3. This situation is similar to the intermediate phase of the extended Hubbard model study of Ref. 53, where similar continuously varying exponents were shown to exist in the metallic non-Fermi-liquid phase in which there was a quenched spin degree of freedom and an unquenched charge degree of freedom. Notice that at $n_d = 3$ only the large-spin state is possible; hence the orbital degrees of freedom are gapped, and exponents disappear, while the effect is maximal one unit of charge away from half filling, i.e., at $n_d = 2$.

IV. CONCLUSIONS

In conclusion, we have shown in this paper that the Hund's rule coupling has a strong impact on the electronic states at valence of one unit of charge away from half filling. The strongly correlated state in such materials can have a very low coherence temperature, and the self-energy and optical conductivity show fractional power-law behavior at intermediate energy. We have derived the effective low-energy Hamiltonian describing these systems and identified a negative Kondo coupling in the spin-spin part of the corresponding low-energy Kondo model. We have shown that these anomalies are not controlled by the proximity to a quantum critical point but result from coexistence of fast quantum mechanical orbital fluctuations and slow spin fluctuations. This is relevant for ruthenates and iron chalcogenides, as well as many other materials with similar valence and sizable Hund's coupling.

ACKNOWLEDGMENTS

We thank Dimitri Basov, Antoine Georges, Jernej Mravlje, Philipp Werner, and Andrew Millis for fruitful discussions. Z.P.Y. and G.K. were supported by NSF Grant No. DMR-0906943; K.H. was supported by NSF Grant No. DMR-0746395.

APPENDIX

1. Schrieffer-Wolff transformation

We start our discussion with the three-band Hubbard model $H = H_t + H_U$, with the hopping term

$$H_t = \sum_{ij\sigma,a,b} t_{ab}^{ij} f_{ia\sigma}^\dagger f_{jb\sigma} \tag{A1}$$

and the Coulomb repulsion term

$$H_U = \frac{1}{2} \sum_{i\sigma,abcd} U[a,b,c,d] f_{ia\sigma}^\dagger f_{ib\sigma'}^\dagger f_{ic\sigma'} f_{id\sigma}. \tag{A2}$$

Here the index a runs over the three orbitals, i,j over lattice sites, and σ over spin. The hopping term is taken to be locally SU(6) symmetric, while the Coulomb interaction is set to $U[a,b,c,d] = U\delta_{ad}\delta_{bc} + J\delta_{ac}\delta_{bd}$, which reduces the symmetry to SU(3) × SU(2).

Within the dynamical mean-field theory, this model maps to the SU(3) × SU(2) impurity Hamiltonian of the form $H_{\rm imp} = H_{\rm bath} + H_{\rm hyb} + H_{\rm local}$,

$$H_{\rm bath} = \sum_{\mathbf{k}a\sigma} \varepsilon_{\mathbf{k}a} \psi_{\mathbf{k}a\sigma}^\dagger \psi_{\mathbf{k}a\sigma}, \tag{A3}$$

$$H_{\rm hyb} = \sum_{\mathbf{k}a\sigma} V_{\mathbf{k}a} \psi_{\mathbf{k}a\sigma}^\dagger f_{a\sigma} + \text{H.c.}, \tag{A4}$$

$$H_{\rm local} = \sum_{a\sigma} \varepsilon_f f_{a\sigma}^\dagger f_{a\sigma} + H_U. \tag{A5}$$

To gain further insights into the low-energy degrees of freedom of this Hamiltonian, we perform the Schrieffer-Wolff transformation, which takes the form

$$H_{\rm eff} = P_n H_{\rm hyb} \frac{P_{n\pm1}}{\Delta E} H_{\rm hyb} P_n, \tag{A6}$$

where P_n is the projector to the impurity ground-state multiplet, and ΔE is the energy cost for the charge excitation from the ground-state multiplet to the $n \pm 1$ lowest-energy multiplet states, and is always negative.

Here we will limit our discussion to the case of a ground-state valence $n_f = 2$ and virtual charge excitations into valence $n_f = 3$. A direct way of evaluating this effective Hamiltonian is to perform exact diagonalization of $H_{\rm local}$, then express matrix elements of $f_{a\sigma}$ operators in terms of atomic eigenstates $(F_{a\sigma}^\dagger)_{m_1m_2} = \langle m_1 | f_{a\sigma}^\dagger | m_2 \rangle$, and finally evaluate all terms which appear in the sum

$$H_{\rm eff} = \sum_{\mathbf{k}\mathbf{k}'ab\sigma\sigma'} \frac{V_{\mathbf{k}a} V_{\mathbf{k}'b}^*}{\Delta E} \psi_{\mathbf{k}a\sigma}^\dagger \psi_{\mathbf{k}'b\sigma'} \times \sum_{m_1m_2m_3} (F_{a\sigma})_{m_1m_2} (F_{b\sigma'}^\dagger)_{m_2m_3} |m_1\rangle\langle m_3|. \tag{A7}$$

Here m_2 runs over the ground-state multiplet at valence $n+1$, while m_1 and m_3 run over the ground-state multiplet at valence n. Finally we need to express the impurity degrees of freedom in terms of the impurity operators such as the total spin S and the orbital isospin operator T.

This tedious derivation can be circumvented by a trick. We Fourier-transform the bath operators $V^2 \psi_{a\sigma}^\dagger(0) = \sum_{\mathbf{k}} V_{\mathbf{k}a} \psi_{\mathbf{k}a\sigma}^\dagger$ and introduce the combined spin-orbit index $i \equiv (a\sigma)$. We can then rewrite the effective Hamiltonian for charge excitations from valence n to valence $n+1$ as

$$H_{\rm eff} = \sum_{ijkl} \frac{V^2}{\Delta E} \psi_i^\dagger(0) \psi_j(0) P_n f_k P_{n+1} f_l^\dagger P_n \ \delta(i,k)\delta(j,l). \tag{A8}$$

We next find a complete orthonormal basis in the space of spin and orbit degrees of freedom [$\text{Tr}(I^\alpha I^{\beta\dagger}) = \delta_{\alpha\beta}$], in which the completeness relation takes the form

$$\delta(i,k)\delta(j,l) = \sum_\alpha (I^{\alpha *})_{ij} (I^\alpha)_{kl}. \tag{A9}$$

Here the matrices I^α form a complete basis for the SU(3) × SU(2) group. For the SU(2) and SU(3) groups we use Pauli 2 × 2 matrices σ^α, and Gell-Mann 3 × 3 matrices λ^α. In terms of these, the complete basis I^α is

$$I^\alpha = \begin{cases} \frac{1}{\sqrt{3}} 1 \otimes 1 \frac{1}{\sqrt{2}}, \\ \frac{1}{\sqrt{3}} 1 \otimes \sigma \frac{1}{\sqrt{2}}, \\ \frac{1}{\sqrt{2}} \lambda \otimes 1 \frac{1}{\sqrt{2}}, \\ \frac{1}{\sqrt{2}} \lambda \otimes \sigma \frac{1}{\sqrt{2}}. \end{cases} \tag{A10}$$

The normalization factors come from the fact that $\mathrm{Tr}(\sigma^\alpha\sigma^\beta) = 2\delta(\alpha,\beta)$ and $\mathrm{Tr}(\lambda^\alpha\lambda^\beta) = 2\delta(\alpha,\beta)$. We can then simplify the low-energy Hamiltonian as

$$H_{\mathrm{eff}} = \sum_{ijkl,\alpha} \frac{V^2}{\Delta E}(I^\alpha)_{kl}\ P_n f_k P_{n+1} f_l^\dagger P_n\ \psi_i^\dagger(0)(I^{\alpha *})_{ij}\psi_j(0). \tag{A11}$$

Next we realize that even in the presence of an arbitrary projector, the local operators keep the same form of the expansion in terms of the electron field operator

$$\sum_{kl}(1\otimes\sigma^\alpha)_{kl}\ P_n f_k P_{n+1} f_l^\dagger P_n \propto -S^\alpha, \tag{A12}$$

$$\sum_{kl}(\lambda^\alpha\otimes 1)_{kl}\ P_n f_k P_{n+1} f_l^\dagger P_n \propto -T^\alpha, \tag{A13}$$

$$\sum_{kl}(\lambda^\alpha\otimes\sigma^\beta)_{kl}\ P_n f_k P_{n+1} f_l^\dagger P_n \propto -T^\alpha\otimes S^\beta, \tag{A14}$$

but the proportionality constants need to be determined by an explicit calculation. Notice that just as in the Wigner-Eckart theorem, we need to consider only one matrix element to determine the proportionality constant, which greatly simplifies this derivation.

Now we can recognize that the first term in Eq. (A10) gives rise to potential scattering of the form

$$H_0 = J_p \sum_{a\sigma}\psi_{a\sigma}^\dagger(0)\psi_{a\sigma}(0), \tag{A15}$$

the second term in Eq. (A10) gives the spin-Kondo part

$$H_1 = J_1 \sum_\alpha S^\alpha \sum_{a\sigma\sigma'}\psi_{a\sigma}^\dagger(0)\sigma^\alpha{}_{\sigma\sigma'}\psi_{a\sigma'}(0), \tag{A16}$$

the third gives the orbital-Kondo part

$$H_2 = J_2 \sum_a T^a \sum_{\alpha\sigma\beta}\psi(0)_{\alpha\sigma}^\dagger\lambda^a_{\alpha,\beta}\psi(0)_{\beta\sigma}, \tag{A17}$$

and the last gives the spin-orbit Kondo part

$$H_3 = J_3 \sum_{a,b} T^a\otimes S^b \sum_{\alpha\sigma\beta}\psi(0)_{\alpha\sigma}^\dagger\lambda^a_{\alpha,\beta}\sigma^b_{\sigma,\sigma'}\psi(0)_{\beta\sigma'} \tag{A18}$$

The Kondo couplings J_1, J_2, J_3 depend on the valence n_f and type of the projector P. We first consider the SU(6)-symmetric case, which is realized in the absence of Hund's rule coupling. In this case, the projector P is irrelevant, since all states at some valence have equal energy. The local operators are then simply given by

$$\sum_{a\sigma\sigma'} f_{a\sigma}\sigma^\alpha_{\sigma\sigma'} f^\dagger_{a\sigma'} = -2S^\alpha,$$

$$\sum_{ab\sigma} f_{a\sigma}\lambda^\alpha_{ab} f^\dagger_{b\sigma'} = -T^\alpha,$$

$$\sum_{ab\sigma\sigma'} f_{a\sigma}\lambda^\alpha_{ab}\sigma^\beta_{\sigma\sigma'} f^\dagger_{b\sigma'} = -2T^\alpha S^\beta,$$

and the Kondo couplings become $J_1 = 2/6\ J_0 = J_0/3$, $J_2 = J_0/4$, and $J_3 = 2/4\ J_0$, where $J_0 = \frac{V^2}{2U+\varepsilon_f} > 0$. Notice that all Kondo couplings are positive (the minus sign comes from ΔE and from the proportionality constant) and hence antiferromagnetic couplings ensure complete quenching of the spin and orbital moments. The ground state is thus a Fermi liquid.

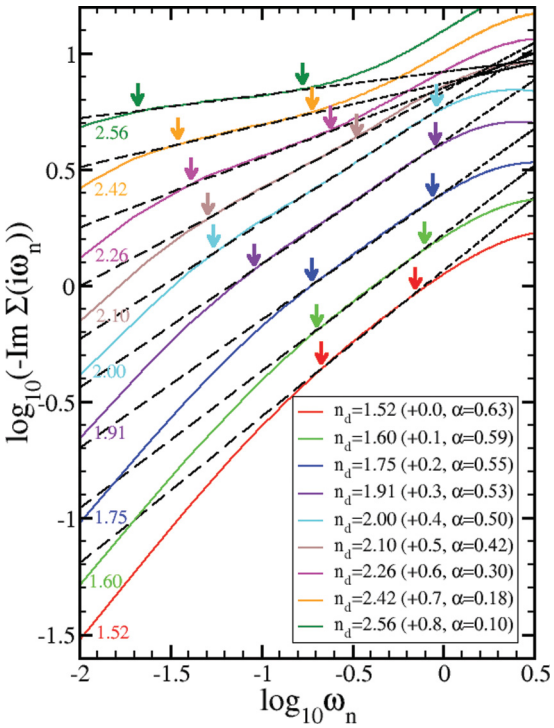

FIG. 5. (Color online) Quasiparticle self energy for $J_H = 2.0$. The imaginary part of the quasiparticle self-energy in the $\log_{10}$-$\log_{10}$ scale as a function of electron occupation n_d for $U = 6.0$ and $J_H = 2.0$. Note the data are shifted along the y axis for better illustration. The linear dispersion of the self-energy in the plot indicates that power-law behavior exists in the intermediate frequency region as indicated by the arrows.

In the limit of large Hund's coupling, the projector P_{n+1} projects to the subspace of high-spin states only, which in the case of the three-band model and $n_f = 3$, take the following forms:

$$|1\rangle \equiv |\downarrow\downarrow\downarrow\rangle, \tag{A19}$$

$$|2\rangle \equiv \frac{1}{\sqrt{3}}(|\downarrow\downarrow\uparrow\rangle + |\downarrow\uparrow\downarrow\rangle + |\uparrow\downarrow\downarrow\rangle), \tag{A20}$$

$$|3\rangle \equiv \frac{1}{\sqrt{3}}(|\downarrow\uparrow\uparrow\rangle + |\uparrow\downarrow\uparrow\rangle + |\uparrow\uparrow\downarrow\rangle), \tag{A21}$$

$$|4\rangle \equiv |\uparrow\uparrow\uparrow\rangle. \tag{A22}$$

Projection to the ground state multiplet P_n is achieved by projecting to the following states:

$$|5\rangle \equiv |\downarrow 0\downarrow\rangle, \tag{A23}$$

$$|6\rangle \equiv |0\downarrow\downarrow\rangle, \tag{A24}$$

$$|7\rangle \equiv |\downarrow\downarrow 0\rangle, \tag{A25}$$

$$|8\rangle \equiv \frac{1}{\sqrt{2}}(|\downarrow 0\uparrow\rangle + |\uparrow 0\downarrow\rangle), \tag{A26}$$

$$|9\rangle \equiv \frac{1}{\sqrt{2}}(|0\downarrow\uparrow\rangle + |0\uparrow\downarrow\rangle), \tag{A27}$$

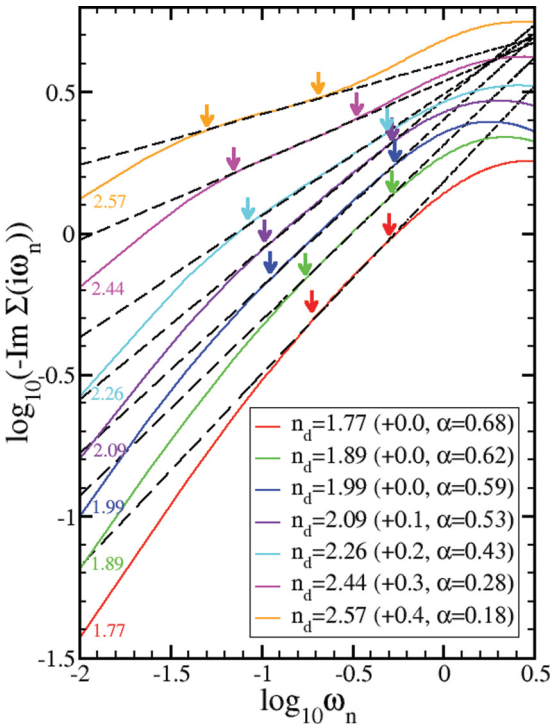

FIG. 6. (Color online) Quasiparticle self-energy for $J_H = 1.0$. The imaginary part of the quasiparticle self-energy in the $\log_{10}$-$\log_{10}$ scale as a function of electron occupation n_d for $U = 6.0$ and $J_H = 1.0$. Note that the data are shifted along the y axis for better illustration. The linear dispersion of the self-energy in the plot indicates that power-law behavior exists in the intermediate frequency region as indicated by the arrows.

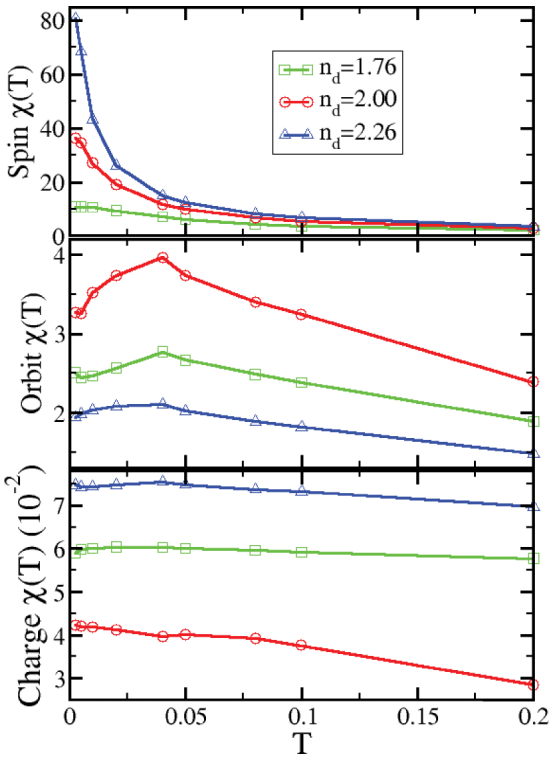

FIG. 7. (Color online) Local spin, orbital, and charge susceptibilities at zero frequency as functions of temperature for $n_d = 1.75$, 2.00, 2.26 and $U = 6.0$, $J_H = 2.0$. The spin susceptibility has large static values and takes the Curie-Weiss form while the orbital susceptibility is Pauli-like and enhanced at intermediate temperature and around $n_d = 2.0$. Note that the charge susceptibility is two orders of magnitude smaller than the orbital susceptibility and thus does not play an important role.

$$|10\rangle \equiv \frac{1}{\sqrt{2}}(|\downarrow\uparrow 0\rangle + |\uparrow\downarrow 0\rangle), \tag{A28}$$

$$|11\rangle \equiv |\uparrow 0\uparrow\rangle, \tag{A29}$$

$$|12\rangle \equiv |0\uparrow\uparrow\rangle, \tag{A30}$$

$$|13\rangle \equiv |\uparrow\uparrow 0\rangle. \tag{A31}$$

An explicit calculation can be used to determine the proportionality constants:

$$\sum_{a\sigma\sigma'} P_n f_{a\sigma}\sigma^{\alpha}_{\sigma\sigma'} P_{n+1} f^{\dagger}_{a\sigma'} P_n = \frac{2}{3}S^{\alpha},$$

$$\sum_{ab\sigma} P_n f_{a\sigma}\lambda^{\alpha}_{ab} P_{n+1} f^{\dagger}_{b\sigma'} P_n = -\frac{4}{3}T^{\alpha},$$

$$\sum_{ab\sigma\sigma'} P_n f_{a\sigma}\lambda^{\alpha}_{ab}\sigma^{\beta}_{\sigma\sigma'} P_{n+1} f^{\dagger}_{b\sigma'} P_n = -\frac{4}{3}T^{\alpha}S^{\beta}.$$

We can finally determine the Kondo couplings in the limit of large Hund's coupling. Their value is $J_1 = -2/3 \times 1/6 J_0 = -J_0/9$, $J_2 = 4/3 \times 1/4 J_0 = J_0/3$, and $J_3 = 4/3 \times 1/4 J_0 = J_0/3$. Here $J_0 = \frac{V^2}{2U-2J_H+\varepsilon_f} > 0$.

The crucial result of this calculation is that the spin-spin Kondo coupling J_1 changes sign when Hund's coupling is strong. This comes from the fact that the spin operator in the projected subspace $\sum_{a\sigma\sigma'} P_n f_{a\sigma}\sigma^{\alpha}_{\sigma\sigma'} P_{n+1} f^{\dagger}_{a\sigma'} P_n = \frac{2}{3}S^{\alpha}$ has very different expansion in terms of the electron field operator than in the nonprojected case $\sum_{a\sigma\sigma'} f_{a\sigma}\sigma^{\alpha}_{\sigma\sigma'} f^{\dagger}_{a\sigma'} = -2S^{\alpha}$. The origin of this sign change is in the orbital blocking mechanism, which ensures that the intermediate state at $n_f = 3$ is a high-spin state (in this case $S = 1$) but is orbitally a singlet state, such as states (A19)–(A22). Orbital blocking is a restriction in the Hilbert space imposed by large Hund's rule coupling. It modifies the Kondo couplings away from their SU(N) symmetric values ($J_1 = J_0/3$, $J_2 = J_0/4$, $J_3 = J_0/2$). This blocking results in different Kondo couplings in different valences. For the half-filled shell (relevant for Mn^{2+}) it results in $J_2 = 0$, $J_3 = 0$, and a strong reduction of the value of J_1, first recognized by Schrieffer.[2] For the valence of one unit of charge away from half-filling (relevant for Fe^{2+} and Ru^{4+}), orbital blocking results in the sign reversal of J_1.

2. Results for the three-band Hubbard model

Using our numerical quantum Monte Carlo methods, we cannot obtain high-precision real axis self-energies; however, we can infer its analytic properties from imaginary-axis analogs. The fractional exponent in the scattering rate on the real axis [$\mathrm{Im}\Sigma(\omega) \propto \omega^{\alpha}$] leads to the same power law on the imaginary axis for the imaginary part [$\mathrm{Im}\Sigma(i\omega_n) \propto -\omega_n^{\alpha}$]. The real part, on the other hand, shows the power law only when the scattering rate is very asymmetric around

zero frequency. For example, for $\Sigma''(\omega > 0) = A|x|^{\alpha}$ and $\Sigma''(\omega < 0) = B|x|^{\alpha}$, the real part on the imaginary axis is $\mathrm{Re}\Sigma(i\omega_n) \propto (A - B)\int_0^{\Lambda} x|x|^{\alpha}/(x^2 + \omega_n^2)dx$ (where Λ is the upper cutoff for the power law), and does not show power-law behavior in the symmetric $A = B$ case. Our calculation shows that the real part does not show a very clear power law on the imaginary axis; hence we infer that the scattering rate is quite symmetric at low frequency on the real axis.

Figure 5 and 6 show the imaginary part of the quasiparticle self-energy in the $\log_{10}$-$\log_{10}$ scale as a function of electron occupation n_d for $U = 6.0$ and $J_H = 2.0$ and 1.0, respectively. The linear dispersion of the self-energy in the plots indicates that power-law behavior exists in the intermediate frequency region as indicated by the arrows. For both values of J_H, the power-law exponent α decreases monotonically with increasing n_d towards half filling, i.e., $n_d = 3$. The upper energy cutoff ε_1^* drops rapidly for $n_d > 2.0$, suggesting that the power-law behavior is vanishing quickly when n_d goes away from 2 to half filling. Compared to the power-law behavior for $J_H = 2.0$, that for $J_H = 1.0$ is valid in a smaller frequency region and the corresponding power-law exponent is larger, suggesting the important role of Hund's coupling in giving rise to the power-law behavior. Therefore the power-law behavior is most visible at electron occupation one unit of charge away from half filling, in this case, $n_d = 2$

Figure 7 shows the local spin, orbital, and charge susceptibilities at zero frequency as a function of temperature for $n_d = 1.75$, 2.00, 2.26 and $U = 6.0$, $J_H = 2.0$. The spin susceptibility has large static values and takes the Curie-Weiss form while the orbital susceptibility is Pauli-like and enhanced at intermediate temperatures and around $n_d = 2.0$. Note that the charge susceptibility is two orders of magnitude smaller than the orbital susceptibility and thus does not play an important role.

*yinzping@physics.rutgers.edu

[1] D. van der Marel and G. A. Sawatzky, Phys. Rev. B **37**, 10674 (1988).
[2] J. R. Schrieffer, J. Appl. Phys. **38**, 1143 (1967).
[3] I. Okada and K. Yosida, Prog. Theor. Phys. **49**, 1483 (1973).
[4] A. Georges, G. Kotliar, W. Krauth, and M. J. Rozenberg, Rev. Mod. Phys. **68**, 13 (1996).
[5] K. Haule and G. Kotliar, New J. Phys. **11**, 025021 (2009).
[6] M. M. Qazilbash *et al.*, Nat. Phys. **5**, 647 (2009).
[7] Z. G. Chen, R. H. Yuan, T. Dong, and N. L. Wang, Phys. Rev. B **81**, 100502(R) (2010).
[8] L. Degiorgi, New J. Phys. **13**, 023011 (2011).
[9] A. A. Schafgans, S. J. Moon, B. C. Pursley, A. D. LaForge, M. M. Qazilbash, A. S. Sefat, D. Mandrus, K. Haule, G. Kotliar, and D. N. Basov, Phys. Rev. Lett. **108**, 147002 (2012).
[10] Z. P. Yin, K. Haule, and G. Kotliar, Nat. Mater. **10**, 932 (2011).
[11] K. Haule, J. H. Shim, and G. Kotliar, Phys. Rev. Lett. **100**, 226402 (2008).
[12] Z. P. Yin, K. Haule, and G. Kotliar, Nat. Phys. **7**, 294 (2011).
[13] M. D. Johannes and I. I. Mazin, Phys. Rev. B **79**, 220510(R) (2009).
[14] G. T. Wang, Y. M. Qian, G. Xu, X. Dai, and Z. Fang, Phys. Rev. Lett. **104**, 047002 (2010).
[15] P. Hansmann, R. Arita, A. Toschi, S. Sakai, G. Sangiovanni, and K. Held, Phys. Rev. Lett. **104**, 197002 (2010).
[16] S. Zhou and Z. Q. Wang, Phys. Rev. Lett. **105**, 096401 (2010).
[17] W.-G. Yin, C.-C. Lee, and W. Ku, Phys. Rev. Lett. **105**, 107004 (2010).
[18] A. Liebsch, Phys. Rev. B **84**, 180505 (2011).
[19] E. Abrahams and Q. Si, J. Phys.: Condens. Matter **23**, 223201 (2011).
[20] L. Craco, M. S. Laad, and S. Leoni, Phys. Rev. B **84**, 224520 (2011).
[21] T. Schickling, F. Gebhard, J. Bunemann, L. Boeri, O. K. Andersen, and W. Weber, Phys. Rev. Lett. **108**, 036406 (2012).
[22] J. Ferber, K. Foyevtsova, R. Valentí, and H. O. Jeschke, Phys. Rev. B **85**, 094505 (2012).
[23] T. Misawa, K. Nakamura, and M. Imada, Phys. Rev. Lett. **108**, 177007 (2012).
[24] N. L. Wang *et al.*, J. Phys.: Condens. Matter **24**, 294202 (2012).
[25] W.-C. Lee and P. W. Phillips, arXiv:1110.5917.
[26] W.-G. Yin, C.-C. Lee, and W. Ku, Supercond. Sci. Technol. **25**, 084007 (2012).
[27] P. Werner, E. Gull, M. Troyer, and A. J. Millis, Phys. Rev. Lett. **101**, 166405 (2008).
[28] T. Katsufuji, M. Kasai, and Y. Tokura, Phys. Rev. Lett. **76**, 126 (1996).
[29] Y. S. Lee, J. S. Lee, T. W. Noh, D. Y. Byun, K. S. Yoo, K. Yamaura, and E. Takayama-Muromachi, Phys. Rev. B **67**, 113101 (2003).
[30] J. Mravlje, M. Aichhorn, T. Miyake, K. Haule, G. Kotliar, and A. Georges, Phys. Rev. Lett. **106**, 096401 (2011).
[31] L. de' Medici, J. Mravlje, and A. Georges, Phys. Rev. Lett. **107**, 256401 (2011).
[32] A. Kutepov, K. Haule, S. Y. Savrasov, and G. Kotliar, Phys. Rev. B **82**, 045105 (2010).
[33] G. Kotliar *et al.*, Rev. Mod. Phys. **78**, 865 (2006).
[34] K. Haule, C.-H. Yee, and K. Kim, Phys. Rev. B **81**, 195107 (2010).
[35] K. Haule, Phys. Rev. B **75**, 155113 (2007).
[36] P. Werner, A. Comanac, L. de Medici, M. Troyer, and A. J. Millis, Phys. Rev. Lett. **97**, 076405 (2006).
[37] T. Vogt and D. J. Buttrey, Phys. Rev. B **52**, 9843(R) (1995).
[38] M. Tropeano *et al.*, Supercond. Sci. Technol. **23**, 054001 (2010).
[39] P. Zavalij *et al.*, Phys. Rev. B **83**, 132509 (2011).
[40] D. Phelan, J. N. Millican, E. L. Thomas, J. B. Leao, Y. Qiu, and R. Paul, Phys. Rev. B **79**, 014519 (2009).
[41] D. N. Basov *et al.*, Rev. Mod. Phys. **83**, 471 (2011).
[42] C. Mirri, P. Calvani, F. M. Vitucci, A. Perucchi, K. W. Yeh, M. K. Wu, and S. Lupi, Supercond. Sci. Technol. **25**, 045002 (2012).
[43] N. Stojilovic, A. Koncz, L. W. Kohlman, R. Hu, C. Petrovic, and S. V. Dordevic, Phys. Rev. B **81**, 174518 (2010).
[44] Z. Fisk *et al.*, Science **239**, 33 (1988).

[45]F. Reinert, D. Ehm, S. Schmidt, G. Nicolay, S. Hufner, J. Kroha, O. Trovarelli, and C. Geibel, Phys. Rev. Lett. **87**, 106401 (2001).
[46]T. Valla *et al.*, Nature (London) **417**, 627 (2002).
[47]M. Aichhorn, S. Biermann, T. Miyake, A. Georges, and M. Imada, Phys. Rev. B **82**, 064504 (2010).
[48]M. Yi *et al.*, arXiv:1208.5192.
[49]T. T. Ong and P. Coleman, Phys. Rev. Lett. **108**, 107201 (2012).
[50]J. W. Simonson *et al.*, Proc. Natl. Acad. Sci. USA **109**, E1815 (2012).
[51]A. H. Nevidomskyy and P. Coleman, Phys. Rev. Lett. **103**, 147205 (2009).
[52]P. Werner *et al.*, Nat. Phys. **8**, 331 (2012).
[53]Q. Si and G. Kotliar, Phys. Rev. Lett. **70**, 3143 (1993).